J Mater Sci (2008) 43:7457–7464
DOI 10.1007/s10853-008-2634-x

ULTRAFINE-GRAINED MATERIALS

Solid-state amorphization of Cu + Zr multi-stacks by ARB and HPT techniques

Y. F. Sun · Y. Todaka · M. Umemoto · N. Tsuji

Received: 3 March 2008 / Accepted: 4 April 2008 / Published online: 13 July 2008

Abstract A series of CuZr binary alloys with wide composition range were fabricated through ARB and HPT techniques using pure Cu and Zr metals as the starting materials. Bulk alloy sheets with thickness of about 0.8 mm after ARB process and alloy disks with 0.30 mm in thickness and 10 mm in diameter after HPT process can be obtained, respectively. The structures of all the alloys were found to be gradually refined with the increase of ARB cycles or HPT rotations. As a result, nanoscale multiple-layered structure was formed for the 10 cycled ARBed specimens, which could partially transform into amorphous phase during subsequent low temperature annealing. While for the as-HPTed sample, the alloy was completely amorphized after 20 rotations without any heat treatment. The thermal stabilities of the amorphous alloys were studied. The deformation behavior and the amorphization mechanism during the ARB and HPT process were put forward and discussed.

Introduction

Amorphous alloys are materials with long range disordered atomic configuration, which often present unique properties and keep on drawing great attention from more and more researchers. Many processing methods including rapid melt quenching, vapor deposition on cold substrates, or mechanical alloying have been invented for the fabrication of amorphous alloys [1, 2]. In the last several decades, various severe plastic deformation (SPD) processes for achieving grain refinement have been developed, such as accumulative roll bonding (ARB), high pressure torsion (HPT), or equal channel angular pressing (ECAP) [3–5]. SPD techniques originally are used to produce bulk nanostructured metallic materials. During the SPD process, bulk materials are subjected to a very intense plastic deformation without significant changes in the overall dimensions. Up to now, a lot of metallic materials such as steel, pure elemental metals including Cu, Ni, Al, and Mg, etc. with nanoscaled grain size have been fabricated, which exhibit high strength and other superior properties. Since intense plastic strain is induced into the SPDed materials, mechanical alloying or even strain-induced solid-state amorphization might take place. Recently, it was found that some alloys with good glass forming ability (GFA) such as Zr–Ti, Cu–Zr, and Zr–Al–Ni–Cu have been amorphized in solid state by repeated cold-rolling [6–12]. While partial amorphization of NiTi, Cu–Zr–Ti, and Nd(Pr)–Fe–B alloys by HPT have also been observed and exhibit well-improved properties [13–16]. However, in the previous work, only amorphous phase with low volume fraction or amorphous phase formed at the grain boundary could be generated due to low HPT rotations or low total equivalent strain. Besides, comparing with the amorphous transformation from their crystalline alloys, solid-state amorphization of alloys from pure metals by means of HPT technique has not been reported so far.

Cu–Zr system is well-known to be favorable for glass forming either by rapid quenching or by the solid-state amorphization [17]. In this paper, two kinds of SPD techniques, namely ARB and HPT, were used for the solid-

Y. F. Sun · N. Tsuji (✉)
Department of Adaptive Machine Systems, Osaka University, Suita, Japan
e-mail: tsuji@ams.eng.osaka-u.ac.jp

Y. Todaka · M. Umemoto
Department of Production Systems Engineering, Toyohashi University of Technology, Toyohashi, Japan

state amorphization of bulk CuZr multi-stacks with overall composition covering wide range. The microstructure evolution and phase transformation during the amorphization process were studied and the mechanism for the formation of amorphous phase were put forward and discussed.

Experimental procedure

In this paper, pure Cu (99.96% purity) and pure Zr (99.2% purity) sheets with 200 mm in length and 50 mm in width were used as starting materials for the ARB process. Several Cu and Zr sheets were alternatively stacked together after degreasing and wire-brushing the sheets surfaces. Then the stacked sheets were first roll-bonded with a reduction in thickness of 75%, corresponding to an equivalent strain of 1.6. The obtained roll-bonded sheets therefore have a multilayered structure. They were then cut into three or four parts, degreased, wire-brushed, stacked, and then roll-bonded again as another cycle. The total ARB process was repeated up to 10 cycles and all the ARB process was carried out at room temperature. By changing the number and thickness of the metal sheets, samples with arbitrary overall compositions can be obtained. In the present study, CuZr multilayers with different composition, namely Cu–29at%Zr, Cu–38at%Zr, and Cu–47at%Zr were prepared. Detailed information about the material can be found in Table 1. The difference of the final equivalent strain was attributed to the different original sheet thickness and the different number of parts stacked during the ARB process. The ARBed multilayer was then heat treated at 400 °C for 30 min for the thermally induced amorphization.

For HPT process, disks with diameter of 10 mm were cut off from the first roll-bonded multi-stacks, i.e., one cycle ARBed samples. During the HPT process, the disks were deformed at a rotation speed of 0.2 rpm under an applied pressure of 5 GPa. Various numbers of rotations, namely 0.5, 1, 5, 10, 20, and 50 were completed separately to prepare the samples with different equivalent strains. After HPT process, pancake-like specimen with diameter of 10 mm and thickness of 0.3 mm were obtained. The temperature rises induced by plastic deformation were measured by inserting thermal couples near the sample surface. During the entire HPT process, the maximum temperature rise was less than 10 K due to the low rotation speed, so that the resultant effect on the alloying behavior can be neglected.

The obtained samples were studied by X-ray diffraction (XRD), scanning electron microscopy (SEM) under back-scattered electron (BSE) mode, and transmission electron microscopy (TEM). Differential scanning calorimeter (DSC) was also used to investigate the thermal properties of the samples at a heating rate of 20 K min^{-1} under a flowing argon atmosphere.

Table 1 Thickness and number of the metal sheets used for bulk mechanical alloying by ARB

	Cu–29at%Zr		Cu–38at%Zr		Cu–47at%Zr	
	Cu	Zr	Cu	Zr	Cu	Zr
Number of sheets	5	4	6	5	7	6
Thickness (μm)	200	200	200	300	100	200
Total thickness (mm)	1.8		2.7		1.9	
Final equivalent strain	16		11.7		14.3	

Experimental results

Solid-state amorphization by ARB and annealing

During the ARB process, every individual Cu or Zr layer in the multi-stacked materials will decrease greatly in thickness due to the increasing equivalent strain. The structure evolutions with increasing ARB cycles for all the samples are almost the same, independent of the overall composition. As a typical example, Fig. 1 shows the SEM-BSE micrographs of the Cu–38at%Zr multi-stacks processed to various ARB cycles. The Cu and Zr layer appear in different contrast in the BSE images, i.e., Cu in dark and Zr in bright. For the samples with low cycles, shear bands can be found penetrating through the entire thickness of materials. As a result, many island-like Zr blocks having diamond shapes are formed, which are indicated by an arrow in Fig. 1b. However, after 6 ARB cycles, the deformation in the multilayer becomes rather homogeneous than before. The microstructure of the specimen processed after 6 and 9 ARB cycles are shown in Fig. 1c and d, respectively. No big island-like Zr blocks can be found and the specimen exhibits very fine lamellar structures.

Figure 2 presents the typical TEM image showing the microstructure of the 9 cycles ARBed Cu–29 at%Zr sample. In the figure, parallel-aligned multilayered structure containing elongated Cu and Zr layers can be observed over a large distance. The thickness of each layer was reduced within a range from 10 to 100 nm. For the ARBed Cu–38at%Zr and Cu–47at%Zr samples, similar fine multilayered structures were also observed.

As an SPD process, ARB can transfer large amount of energy to the deformed samples and lead to the possible formation of non-equilibrium phases. To understand the thermal stability of the materials ARB processed with different cycles, DSC measurements were carried out. Figure 3 shows the DSC curves of the samples with various cycles. The change in DSC curves is similar in the three different materials independent of overall compositions.

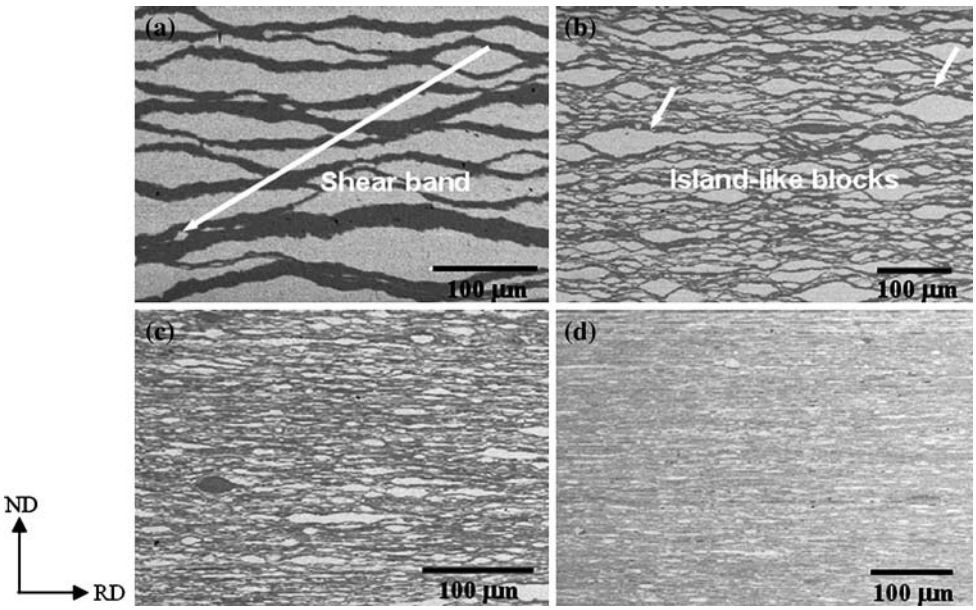

Fig. 1 SEM-BSE micrographs of the Cu–38at%Zr multilayer specimens ARB processed by (**a**) 2 cycles, (**b**) 4 cycles, (**c**) 6 cycles, and (**d**) 9 cycles. Observed from TD

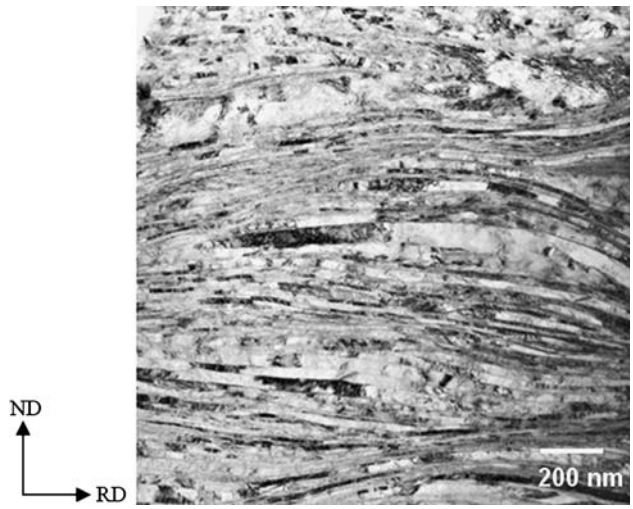

Fig. 2 TEM image showing the microstructure of 9 cycles ARBed Cu–29at%Zr

For 1 cycle ARB processed sample, no obvious endothermic or exothermic reaction can be found on the whole profile. With the increase of ARB cycles, three exothermic peaks begin to appear on the curves and become more and more obvious. For all the 10 cycle ARBed samples, the locations of the exothermic peaks are almost the same and the three peak temperatures are about 665 K, 734 K, and 767 K, respectively. It can be found that this thermal behavior of the ARBed sample is very similar to that of the ball-milled $Cu_{33}Zr_{67}$ powders reported in Ref. [17], in which the first exothermic peak was said to be caused by thermally induced solid-state amorphization.

To actualize the thermally driven amorphization, the 10 cycles ARBed samples were annealed at 673 K in argon atmosphere, which was slightly higher than the first exothermic peak temperature on the DSC curves. After annealing for 30 min, the samples were immediately quenched in water. Figure 4 shows the TEM images of the heat-treated samples, from which it can be found that the microstructures are different depending on the overall compositions. For the Cu–29at%Zr sample, the lamellar structure remains unchanged after heat treatment. However, some layers show gray color and exhibit no contrast inside, which indicate the formation of a non-crystalline structure. From the inserted selected area electronic diffraction (SAED) pattern, a broaden diffraction ring or halo pattern indicating the formation of amorphous phase can be observed, simultaneously with some sharp narrow crystalline diffraction rings. It can be concluded therefore that the gray regions without any contrast in Fig. 4 are amorphous phase formed in the heat treatment. The remaining part was found to be crystalline Cu layers. In Cu–38at%Zr and Cu–47at%Zr sample, much more gray area can be found from the TEM images as shown in Fig. 4b and c. For Cu–38at%Zr, the interface between the neighboring metal layers cannot be discerned any more. From the corresponding SAED pattern, obvious broaden diffraction ring can be found, confirming the existence of amorphous phase. Some crystalline diffraction ring corresponding to Zr layers can still be recognized, but with very weak intensity indicating very small volume fraction in the sample. Similar microstructural characterization can also be seen for Cu–47at%Zr sample. The remaining crystalline Zr layers can be discerned and indicated in Fig. 4c.

The amorphous phase formed upon heat treatment at 673 K of the 10 cycles ARB processed sample was further verified by DSC measurement. Figure 5 shows the DSC

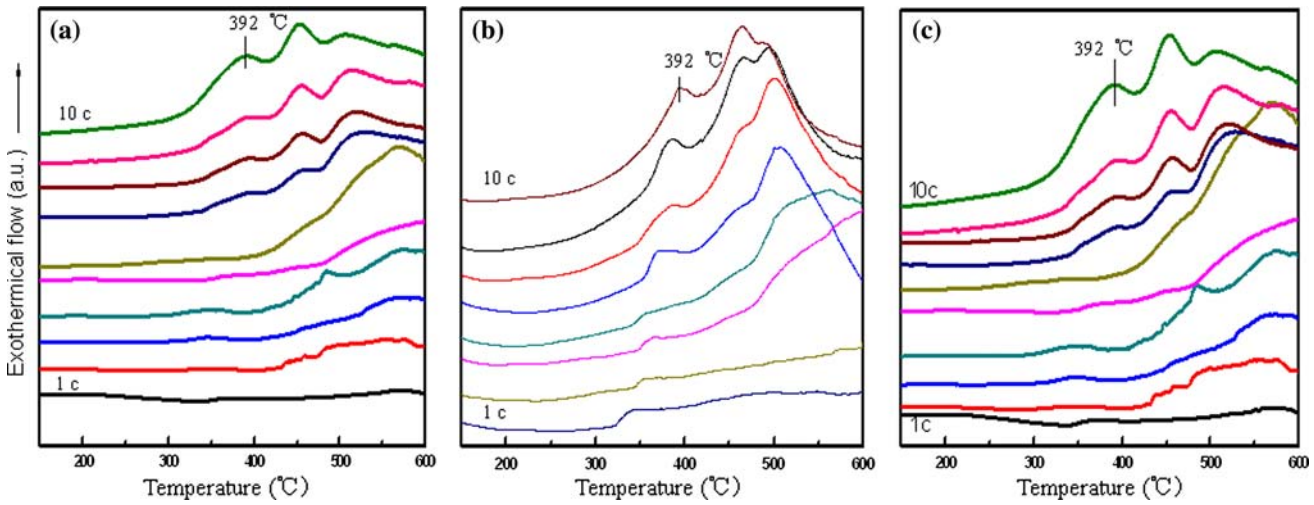

Fig. 3 DSC curves of the Cu–Zr specimens after various ARB cycles (**a**) Cu–29Zr, (**b**) Cu–38Zr, and (**c**) Cu–47Zr

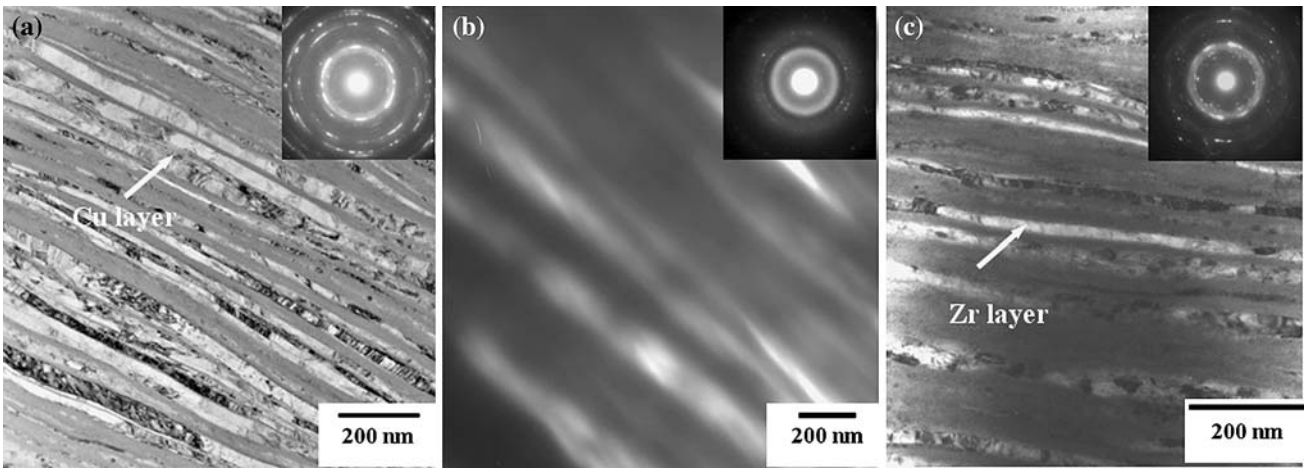

Fig. 4 TEM images showing the microstructure of 10 cycles ARBed (**a**) Cu–29Zr, (**b**) Cu–38Zr, and (**c**) Cu–Zr followed by annealing at 673 K for 30 min

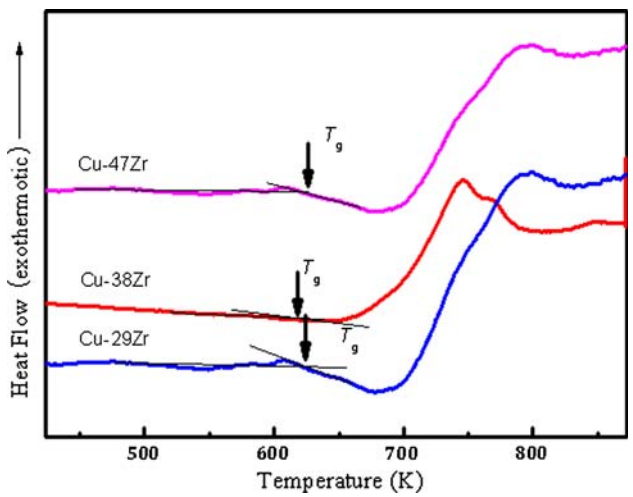

Fig. 5 DSC curves of 10 cycles ARBed CuZr multilayers followed by annealing at 673 K

curves of the ARB processed and heat-treated sample. For all the solid-state amorphorized samples, an obvious endothermic reaction corresponding to glass transition can be found on the curves arrowed as T_g, subsequently followed by a crystallization peak. From the above description, bulk sheets of amorphous/metal nanocomposite could be fabricated by the ARB process followed by heat treatment and the fraction of amorphous phase can be controlled by changing the overall composition of the initial stacks.

Solid-state amorphization by HPT

As a typical example of HPT results, Fig. 6 shows the SEM-BSE image revealing the microstructure evolution of the CuZr specimens with various HPT rotations. The samples for observation were cut into two halves across the

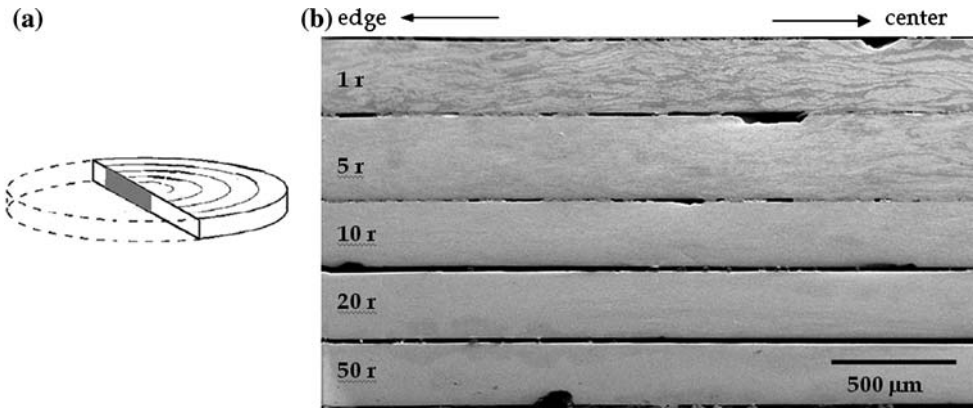

Fig. 6 (**a**) Location of the HPTed sample for SEM observation and (**b**) SEM image of HPTed Cu–47at%Zr samples

center of the materials and were examined on the radial-sectional plane, namely the gray area indicated in Fig. 6a. For all the samples with different overall compositions, the microstructure evolutions were quite similar. That is, the microstructure was refined greatly with increasing HPT rotation number. And the microstructure of the HPTed materials become finer gradually from center to the edge part of the samples, corresponding to the higher equivalent strain in the edge region than that in the center region. However, after 10 rotations, the microstructure become quite homogenous and no contrast can be seen, which reveals that a large extent of atomic mixing of Cu and Zr elements has taken place. For all the samples with various rotations, no fracture or crack can be found at the entire radial-sectional plane, which indicates that the materials exhibit high plasticity during the HPT process.

Figure 7 shows the XRD curves of the CuZr samples with various rotations, revealing the phase transformation during the HPT process. It can be found that the intense of diffraction peak decreases gradually with increasing rotation number, i.e., strain. After five rotations, a broad halo at around $2\theta = 40°$ begins to appear on the curve with some remaining crystalline diffraction peaks. It implies the formation of amorphous phase. After 20 rotations, no sharp diffraction peak but only a broad halo can be found on the curves. From Fig. 8 showing the typical TEM images with the corresponding SAED pattern inserted for the CuZr with 20 rotations, it can further be confirmed that no crystals but only amorphous phase was formed. It should also be pointed out that for the sample with rotations from 0.5 to 50, no diffraction peaks of intermetallic compound can be found on the XRD curves, although they are thermodynamically equilibrium phases. It is supposed that the generation of large amount of crystalline defects like vacancy and dislocations in the HPT process caused the two metals system thermodynamically very unstable. Though the driving force for intermetallic compound should be larger than that for amorphous formation, no intermetallic phase was found in the present HPT samples. A certain degree of atom diffusion is necessary for the nucleation and growth of intermetallic phases. As was mentioned before, the temperature rise in the present HPT

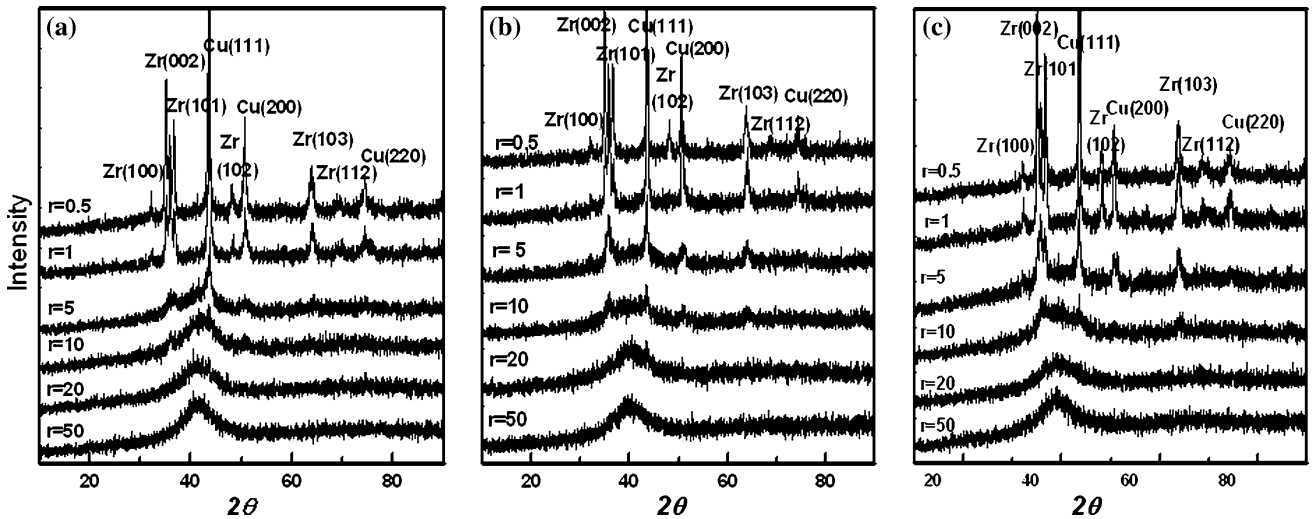

Fig. 7 XRD curves of the HPTed CuZr specimens with various rotations (**a**) Cu–29Zr, (**b**) Cu–38Zr, and (**c**) Cu–47Zr

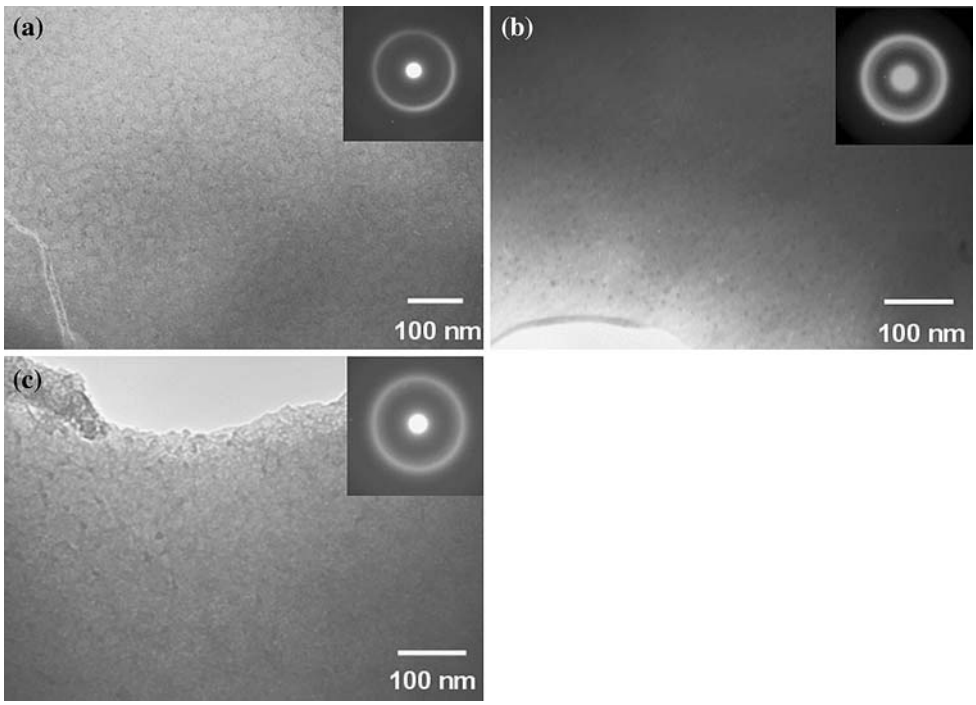

Fig. 8 TEM images of the (**a**) Cu–29Zr, (**b**) Cu–38Zr, and (**c**) Cu–47Zr HPTed specimens with 20 rotations

process was very small because of low rotation speed, so that intermetallic compounds were not formed probably.

Figure 9 shows the DSC curves recorded for the as HPTed samples with various rotations. For the samples with 0.5 and 1 rotation, some weak protuberance can be found on the DSC curves. Since a lot of lattice defects such as dislocations and vacancies must be introduced into the HPTed sample, the protuberance on the DSC curves are supposed to be due to the annihilations of these lattice defects. After five HPT rotations, a sharp exothermic peak begins to appear around 500 °C on the DSC curves. According to the XRD results indicating the formation of amorphous phase after five rotations, the exothermic peak is presumably caused by the crystallization of amorphous phase. However, the glass transition of all the HPTed samples cannot be detected from the DSC curves for the Cu–29at%Zr sample. However, for the Cu–38at%Zr and Cu–47at%Zr samples, obvious T_g and T_x can be observed on the DSC curves after 50 rotations. The glass transition and the crystallization features of the amorphous phases formed by solid-state reaction are almost identical to that formed by rapid quenching methods.

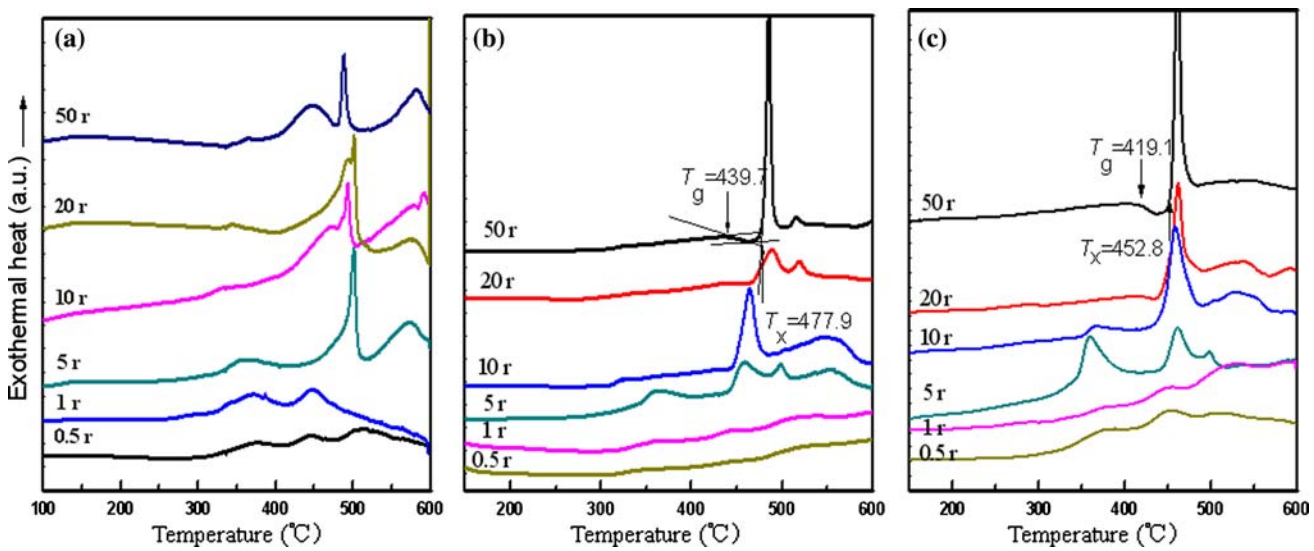

Fig. 9 Thermal stabilities of the HPTed alloys with various HPT rotations (**a**) Cu–29Zr, (**b**) Cu–38Zr, and (**c**) Cu–47Zr

Discussions

In this paper, we can see that partial amorphization of bulk CuZr multi-stacks can be accomplished by ARB process followed by low temperature annealing and monolithic CuZr BMG disks can be obtained by HPT process. The phenomenon of thermally induced amorphization was first discovered in Au-La binary alloys by Schwarz and Johnson in 1983 [18]. Later on, a lot of thermally induced amorphization has been found in electro-deposited films and ball-milled powders [19, 20]. For the thermally induced amorphization, very large interface between the constitutive metals is the most principal factor. Secondly, an atomic radius difference of more than 10% is important for glass formation which will result in anomalous fast diffusion of one element into another. Finally, a negative enthalpy of mixing is said to be favorable for good GFA. For ARBed CuZr multi-stacks with 10 cycles, the multilayered structure makes the structure similar to that of the electro-deposited thin films. Simultaneously, the atomic radium in Cu–Zr system (Cu, 0.128 nm; Zr, 0.161 nm) and negative mixing enthalpy of −23 kJ/mol meet the criteria for thermally induced amorphization. Additionally, to suppress the nucleation and growth of thermodynamically stable intermetallic compounds, the annealing was carried out at temperature much lower than the crystallization peak according to the DSC curve in Fig. 3.

As for stain-induced amorphization, i.e., HPT processed CuZr in this paper, it is supposed that large quantities of lattice defects in the metals caused by intense plastic deformation will greatly accelerate the atomic intermixing rate to achieve a high value of supersaturation, even at room temperature. The supersaturated solid solution will become thermodynamically unstable and transforms to an amorphous phase. In contrast to the thermally driven amorphization occurring between elements that have a strong negative heat of mixing, many strain-induced amorphization has been found to take place between elements providing even positive heat of mixing [Nakamura T, Tsuji N, unpublished data]. The most important factor that dominates the crystal to amorphous transformation seems to be the total equivalent strain or the number of HPT rotations in this study.

It is also important to note that the tendency for glass formation or the GFA of the CuZr alloy depend on the overall composition, which is very similar to that of the solidified CuZr. Binary Cu–Zr alloys fabricated through solidification routes have been studied widely in recent years [21, 22]. It was found that CuZr metallic glass can be obtained in a very wide composition ranged from 25at%Zr to 60at%Zr by means of melt-spinning methods. It is said that the best GFA of CuZr are located in a very narrow composition range. However, the exact composition is controversial. The alloy with composition of $Cu_{60}Zr_{40}$, $Cu_{64.5}Zr_{35.5}$, $Cu_{64}Zr_{36}$, and $Cu_{50}Zr_{50}$ have been said to exhibit the best GFA by different research groups [23–25]. Considering the experimental results in the present study, the samples with composition of Cu–38%atZr and Cu–47%atZr obviously show better GFA than Cu–29%atZr, regardless of the fabrication technique. For the thermally induced amorphization of the ARBed CuZr multi-stack, the volume fraction of the amorphous phase is much less for Cu–29%atZr than those for Cu–38%at Zr and Cu–47%at Zr counterpart, which can be confirmed from the area of the gray regions in Fig. 4. For the HPTed sample, although from XRD and TEM investigation, all the three composition were transformed into monolithic BMG finally after 20 rations, the T_g and T_x transition peak cannot be detected by DSC measurements for Cu–29%atZr. It is supposed that composition inhomogeneity or internal stress still might exist in the Cu–29%at Zr sample even after 50 HPT rotations, which will prevent the detecting of T_g and T_x during the DSC measurements. While for the other two compositions, T_g and T_x can be clearly found on the DSC curves even after 20 HPT rotations.

Conclusions

ARB followed by low temperature heat treatment and HPT techniques can be used for the solid-state amorphization of CuZr system. The following conclusions can be drawn.

a) Thermally induced amorphization can be partially accomplished in the ARBed Cu–Zr multi-stacks by low temperature heat treatment.
b) Monolithic CuZr BMG within wide composition range can be obtained from mixture of pure Cu and Zr metals by HPT process.
c) The tendency of the glass forming by SPD technique is in line with that for the alloys prepared by rapid liquid–solid transformation methods. That is, Cu–38at%Zr and Cu–47%atZr have a better GFA than Cu–29at%Zr, regardless of the technique for the fabrication routes.

Acknowledgement The present study was financially supported by the Grant-in-Aid for Scientific Research on Priority Area "Materials Science of Bulk Metallic Glasses" and the Global COE program "Center of Excellent for Advanced Structural and Functional Materials Design" in Osaka University both through MEXT, Japan.

References

1. Johnson WL (1999) MRS Bull 24:42
2. Chen HS (1980) Rep Prog Phys 43:353. doi:10.1088/0034-4885/43/4/001
3. Valiev RZ, Islamgaliev RK, Alexandrov IV (2000) Prog Mater Sci 45:103. doi:10.1016/S0079-6425(99)00007-9

4. Langdon TG (2006) Rev Adv Mater Sci 11:34
5. Saito Y, Utsunomiya H, Tsuji N (1999) Acta Mater 47:579. doi:10.1016/S1359-6454(98)00365-6
6. Sagel A, Sieber H, Fecht HJ (1998) Acta Mater 46:4233. doi:10.1016/S1359-6454(98)00097-4
7. Wilde G, Rosner H (2007) J Mater Sci 42:1772. doi:10.1007/s10853-006-0986-7
8. Atzmon M, Verhoeven JD, Gibson ED (1984) Appl Phys Lett 45:1052. doi:10.1063/1.95064
9. Hsieh PJ, Huang JC, Hung YP (2004) Mater Chem Phys 88:364. doi:10.1016/j.matchemphys.2004.08.002
10. Ohsaki S, Kato S, Tsuji N (2007) Acta Mater 55:2885. doi:10.1016/j.actamat.2006.12.027
11. Sun YF, Tsuji N, Kato S (2007) Mater Trans 48:1605. doi:10.2320/matertrans.MJ200735
12. Hellstern E, Schultz L (1986) Appl Phys Lett 48:124. doi:10.1063/1.96971
13. Stolyarov VV, Gunderov DV, Popov AG, Gaviko VS, Ermolenko AS (1998) J Alloy Compos 281:69. doi:10.1016/S0925-8388(98)00774-9
14. Sergueeva AV, Song C, Valiev RZ, Mukherjee AK (2003) Mater Sci Eng A 339:159
15. Revesz A, Hobor S, Labar JL, Zhilyaev AP, Kovacs Z (2006) J Appl Phys 100:103522. doi:10.1063/1.2388868
16. Huang JY, Zhu YT, Liao XZ, Valiev RZ (2004) Philos Mag Lett 84(3):183. doi:10.1080/09500830310001657353
17. El-Eskandarany Sherif M, Inoue A (2002) Metal Mater Trans 33:2145. doi:10.1007/s11661-002-0046-0
18. Schwarz RB, Johnson WL (1983) Phys Rev Lett 51:415. doi:10.1103/PhysRevLett.51.415
19. Zhang Q, Lai WS, Yang GW (2002) J Phys Condens Matter 12:6991. doi:10.1088/0953-8984/12/31/301
20. Chu JP, Liu CT, Wang SF (2004) Phys Rev B 69:113410. doi:10.1103/PhysRevB.69.113410
21. Wang D, Li Y, Sun BB (2004) Appl Phys Lett 20:4029. doi:10.1063/1.1751219
22. Xu D, Duan G, Johnson WL (2004) Phys Rev Lett 92:245504. doi:10.1103/PhysRevLett.92.245504
23. Inoue A, Zhang W (2004) Mater Trans 45:584. doi:10.2320/matertrans.45.584
24. Xu D, Lohwongwatana B, Duan G (2004) Acta Mater 52:2621. doi:10.1016/j.actamat.2004.02.009
25. Tang MB, Zhao DQ, Pan MX (2004) Chin Phys Lett 21:901. doi:10.1088/0256-307X/21/4/001